

22. Time-resolved absorption studies have shown conclusively that the single-exponential decay observed by TCSPC spectroscopy corresponds to the ET quenching rate for similar D-bridge-A systems that feature (porphinato)zinc donors and (porphinato)iron acceptors (18, 19).
23. Samples for transient spectroscopic studies were kept rigorously dry with standard inert-atmosphere techniques. The solids were dried overnight under vacuum at 60°C and then dissolved in dry CH₂Cl₂ and transferred under nitrogen to a Schlenk-style fluorescence cell to continuously maintain an inert atmosphere throughout the experiment. Sample concentrations were determined by electronic absorption spectroscopy with use of the known extinction coefficients of the compounds.
24. Although the system is a complex mixture of **4(Zn^{II})** and **4(Fe^{III})** monomers as well as **1(Zn^{II}, Fe^{III})**, **1(Fe^{III}, Fe^{III})**, and **1(Zn^{II}, Zn^{II})** dimers in equilibrium, the analysis is simplified by the facts that (i) **4(Fe^{III})** and **1(Fe^{III}, Fe^{III})** are nonfluorescent and (ii) maintaining a low concentration of **4(Zn^{II})** (35 μM) guarantees that the concentration of ET-inactive **1(Zn^{II}, Zn^{II})** is negligible.
25. The C–O stretching frequencies ν_{CO} for **4(Zn^{II})** and **1(Zn^{II}, Zn^{II})** are 1735 and 1695 cm⁻¹, respectively. The small differences between the K_{assoc} values obtained from the IR (250 M⁻¹) and kinetic studies likely derive from the fact that the IR data were obtained from solutions 2 to 3 orders of magnitude greater in concentration in **4(Zn^{II})** than was used in the TCSPC experiments. Furthermore, for simplicity, **4(Zn^{II})** and **4(Fe^{III})** mixtures were not used in the IR experiments.
26. S. G. DiMugno, V. S.-Y. Lin, M. J. Therien, *J. Am. Chem. Soc.* **115**, 2513 (1993); *J. Org. Chem.* **58**, 5983 (1993); V. S.-Y. Lin, S. G. DiMugno, M. J. Therien, *Science* **264**, 1105 (1994).
27. The synthesis of **2(Zn^{II}, Fe^{III})** and **3(Zn^{II}, Fe^{III})** are reported in P. J. F. de Rege and M. J. Therien, *Inorg. Chim. Acta*, in press.
28. The mixed-metal supramolecular systems used in our ET studies, **2(Zn^{II}, Fe^{III})** and **3(Zn^{II}, Fe^{III})**, were synthesized from **2(Zn^{II}, Zn^{II})** and **3(Zn^{II}, Zn^{II})** by previously reported methods (18, 27). Sample preparation for photophysical studies and analysis of their ET kinetics follow protocols reported in (18).
29. An analogous H-bonding D-A complex **5(Zn^{II}, Fe^{III})** was assembled with [5-(4'-carboxyphenyl)-10,15,20-tris(4''-methoxyphenyl)porphinato]zinc(II), **6(Zn^{II})**, and [5-(4'-carboxyphenyl)-10,15,20-tris(4''-methoxyphenyl)porphinato]iron(III) chloride, **6(Fe^{III})**, as components. The driving force and evaluated ET rate constants were -0.99 eV and $6.2 \times 10^{-9} \text{ s}^{-1}$. Because this ET reaction is more exoergic than those of **2(Zn^{II}, Fe^{III})** and **3(Zn^{II}, Fe^{III})** and because the slightly smaller ET rate constant for **5(Zn^{II}, Fe^{III})** relative to **1(Zn^{II}, Fe^{III})** may derive from the onset of Marcus inverted region effects, we chose **1(Zn^{II}, Fe^{III})** as the benchmark for comparison with **2(Zn^{II}, Fe^{III})** and **3(Zn^{II}, Fe^{III})**. The less exoergic **1(Zn^{II}, Fe^{III})** thus sets a lower limit for relative coupling enhancement provided by a H-bond interface relative to one composed entirely of σ bonds. The evaluated rate constants for the photoinduced ET reactions of both the less exoergic **1(Zn^{II}, Fe^{III})** and the more exoergic **5(Zn^{II}, Fe^{III})** exceed that evaluated for **2(Zn^{II}, Fe^{III})**.
30. Significantly different librational motions of the bridge with respect to D and A can also attenuate electronic coupling. Two such types of motion need to be considered. The first involves librations about the porphyrin-to-phenyl bond that is part of the ET pathway. It is known that the magnitude of electronic coupling follows an approximate $\cos \theta$ dependence, where θ is the dihedral angle between the porphyrin and aryl planes; the fact that single exponential decay is observed in the ET kinetics for such systems reflects a rate constant for the "average" electronic coupling provided by the distribution of angles θ accessible in solution [L. R. Khundkar, J. W. Perry, J. E. Hanson, P. B. Dervan, *J. Am. Chem. Soc.* **116**, 9700 (1994); D. N. Beratan, *ibid.* **108**, 4321 (1986); (18)]. Because the distribution of dihedral angles θ will be the same for compounds **1(Zn^{II}, Fe^{III})**, **2(Zn^{II}, Fe^{III})**, and **3(Zn^{II}, Fe^{III})**, the electronic coupling between the porphyrin and the meso aryl group is invariant. Similarly, the calculated barriers to rotation of the central portion of each bridge with respect to its pendant aryl rings is $\sim 3.0 \text{ kcal mol}^{-1}$ (MOPAC 6.0; J. J. P. Stewart, Frank J. Seiler Research Laboratory, U.S. Air Force Academy). Rotation about the central portion of the bridge is thus similarly fast in all three systems; to first approximation, bridge dynamics cannot account for the observed differences in coupling.
31. R. A. Marcus and N. Sutin, *Biochim. Biophys. Acta* **811**, 265 (1986).
32. S. E. Peterson-Kennedy, J. L. McGourty, J. A. Kalweit, B. M. Hoffman, *J. Am. Chem. Soc.* **108**, 1739 (1986).
33. G. L. Closs and J. R. Miller *Science* **240**, 440 (1988); M. R. Wasielewski, *Chem. Rev.* **92**, 435 (1992).
34. Y. Sakata *et al.*, *Chem. Lett.* **1991**, 1307 (1991); Y. Sakata *et al.*, *J. Am. Chem. Soc.* **111**, 8979 (1989).
35. Recent work by Miller also indicates that the introduction of a C=C double bond into an otherwise saturated bridge leads to enhanced D-A coupling relative to that found for the purely aliphatic ET medium, even when the point of unsaturation is well separated from both D and A (B. P. Paulson, W.-X. Gan, G. L. Closs, J. R. Miller, in preparation).
36. M. R. Wasielewski, M. P. Niemczyk, W. A. Svec, E. B. Pewitt, *J. Am. Chem. Soc.* **107**, 1080 (1985); A. D. Joran *et al.*, *Nature* **327**, 508 (1987); G. L. Gaines III, M. P. O'Neil, W. A. Svec, M. P. Niemczyk, M. R. Wasielewski, *J. Am. Chem. Soc.* **113**, 719 (1991).
37. M. Colapietro and A. Domenicano, *Acta. Crystallogr. B* **38**, 1953 (1982); *ibid.* **34**, 3277 (1978).
38. Driving force (ΔG°) was calculated from appropriate electrochemical parameters and the E_{O-O} values (¹ZnP^{+/}ZnP) for the (porphinato)zinc chromophores, which are defined as the mean of the Q(0, 0) energy and the highest energy emission wavelength (36). For **1(Zn^{II}, Fe^{III})**, electrochemical and photophysical parameters were based on measurements carried out with **4(Fe^{III})** and **4(Zn^{II})**: (ZnP^{+/}ZnP) = 830 mV; (Fe^{III}P/Fe^{II}P) = -560 mV; (¹ZnP^{+/}ZnP) = 2.09 eV. For **2(Zn^{II}, Fe^{III})** and **3(Zn^{II}, Fe^{III})**, electrochemical and photophysical parameters were based on measurements carried out with [5-(4'-methoxyphenyl)-15-(4''-iso-propylphenyl)-10,20-diphenylporphinato]zinc(II) and [5-(4'-methoxyphenyl)-15-(4''-iso-propylphenyl)-10,20-diphenylporphinato]iron(III) chloride, which served as model compounds for the covalent supramolecular ET systems: (ZnP^{+/}ZnP) = 740 mV; (Fe^{III}P/Fe^{II}P) = -490 mV; (¹ZnP^{+/}ZnP) = 2.10 eV. Cyclic voltammetric experimental conditions: [porphyrin] = 1 mM; [TBAPF₆] or [TBAC] = 0.10 M (TBA, tetra-*n*-butylammonium); solvent = CH₂Cl₂; scan rate = 0.5 V s⁻¹; standard calomel reference electrode, 0.1-μm platinum disk working electrode; internal standard = ferrocene/ferrocenium (Fe^{II}/Fe^{III}) redox couple = 430 mV. TBAPF₆ was the supporting electrolyte used in the determination of the ZnP^{+/}ZnP redox couples, whereas TBACI was used as the supporting electrolyte when Fe^{III}P/Fe^{II}P electrochemical potentials were evaluated.
39. Kinetic measurements were performed at the NIH-supported Regional Laser and Biotechnology Laboratory (RLBL) at the University of Pennsylvania. The authors thank L. G. Jahn for his assistance with these measurements. P. J. F. D. thanks the National Science and Engineering Research Council of Canada for a postgraduate fellowship. This work was supported by the Searle Scholars Program (Chicago Community Trust) and the U.S. Department of Energy (DE-FG02-94ER14494). M. J. T. is extremely grateful to the Arnold and Mabel Beckman Foundation, E. I. du Pont de Nemours, and the National Science Foundation for Young Investigator Awards, as well as the Alfred P. Sloan Foundation for a research fellowship.

17 March 1995; accepted 13 July 1995

Synchrony and Causal Relations Between Permian-Triassic Boundary Crises and Siberian Flood Volcanism

Paul R. Renne,* Zhang Zichao, Mark A. Richards, Michael T. Black,† Asish R. Basu

The Permian-Triassic boundary records the most severe mass extinctions in Earth's history. Siberian flood volcanism, the most profuse known such subaerial event, produced 2 million to 3 million cubic kilometers of volcanic ejecta in approximately 1 million years or less. Analysis of ⁴⁰Ar/³⁹Ar data from two tuffs in southern China yielded a date of 250.0 ± 0.2 million years ago for the Permian-Triassic boundary, which is comparable to the inception of main stage Siberian flood volcanism at 250.0 ± 0.3 million years ago. Volcanogenic sulfate aerosols and the dynamic effects of the Siberian plume likely contributed to environmental extrema that led to the mass extinctions.

Continental flood volcanism produced episodic outpourings of magma, chiefly basalt, whose volumes (up to 3.0 × 10⁶ km³) and

mean eruption rates [up to 3 km³/year sustained for ~1 million years (My)] are significantly larger than those of volcanism in other geologic settings (1). Causal relations between flood volcanism and mass extinctions have been postulated for more than a decade (2, 3), in part because of the apparent coincidence between the two most profound mass extinctions known (Permian-Triassic and Cretaceous-Tertiary) and two of the most extensive continental flood volcanism events (Siberian and Deccan traps, respectively). Likely mechanisms of mass mortality (3–5) posed by flood basalts include global cooling caused by sulfate aero-

P. R. Renne and M. T. Black, Berkeley Geochronology Center, 2455 Ridge Road, Berkeley, CA 94709, USA.
Z. Zichao, Yichang Institute of Geology and Mineral Resources, Post Office Box 502, Yichang 443003, People's Republic of China.
M. A. Richards, Department of Geology and Geophysics, University of California, Berkeley, CA 94720, USA.
A. R. Basu, Department of Earth and Environmental Sciences, University of Rochester, Rochester, NY 14627, USA.

*To whom correspondence should be addressed.
†Present address: Department of Biological Anthropology and Anatomy, Duke University, Durham, NC 27706, USA.

sol accumulation and acid rain resulting from reduction and coalescence of sulfates.

The Permian-Triassic (P-T) mass extinctions were the most catastrophic in the geologic record, with as many as 90% of marine species and 70% of terrestrial vertebrate families dying out (6, 7) along with significant floral extinctions (8). Global circumstances attending the extinctions are not well understood. Oxidation of carbon and rapid influx of radiogenic strontium into the oceans most likely resulted from a major sea level drop (regression) that coincided with the extinctions (9, 10). These phenomena are consistent with short-term global cooling and ice cap expansion (11) and also with a pulse of acid rain, as has been inferred at the Cretaceous-Tertiary (K-T) boundary (12). Unlike the K-T boundary, no compelling evidence for a bolide impact at P-T time is known. Although several researchers have inferred a correlation between the P-T boundary and the Siberian traps (10, 11, 13, 14), uncertainty in the age of the boundary has hindered confidence in the correlation. Here, we demonstrate that the two phenomena were synchronous within several hundred thousand years.

The Siberian traps represent the most voluminous known continental flood volcanism in Earth's history, with an original volume estimated at 2×10^6 to 3×10^6 km³ distributed over 2.5×10^6 km² in central Siberia. The traps' volcanic succession overlies Permian strata and is in turn overlaid by Triassic strata (15), although the biostratigraphy is based on sparse terrestrial faunas. The principal magmatic activity was of short duration (~1 My) and occurred about 250 million years ago (Ma) (11, 13, 14, 16, 17). Although the dates reported by various ⁴⁰Ar/³⁹Ar and U-Pb studies range from 243 to 250 Ma, most of this range results from inconsistent use of standards for ⁴⁰Ar/³⁹Ar dating. Renne and Basu (13) reported an age of 248.4 ± 0.3 Ma (2 σ errors here and throughout) for the inception of main-stage Siberian traps volcanism; this age was recalculated to 250.0 ± 1.6 Ma (17) on the basis of astronomical calibration of the age of the Fish Canyon sanidine standard (18). The recalculated age uncertainty is larger because it incorporates uncertainty in the standard's age (18), whereas the previous uncertainty did not reflect this consideration.

The inception age of the Siberian traps (250.0 ± 1.6 Ma) can be compared with the P-T boundary age (251.2 ± 3.4 Ma) obtained by U-Pb ion microprobe analysis of zircons from a bentonitic tuff at the P-T boundary in the Meishan section in Zhejiang Province, southern China (19). On the basis of a critical value test, these two ages can be distinguished from each other at the 48% confidence level. The two dates differ by 1.2

± 3.8 My (2 σ); thus, on the basis of these data, the P-T boundary could have preceded the beginning of Siberian volcanism by as much as 5.0 My or succeeded it by as much as 2.6 My at the 95% confidence level.

To test more rigorously the relative ages of these two events, we used the ⁴⁰Ar/³⁹Ar method to date feldspars from tuffs at the P-T boundary in two different sections in southern China (Fig. 1). These sections are widely believed to contain the most stratigraphically complete P-T sections in the world. Sample C-2 consisted of sanidine grains (100 to 150 μ m across) from a bentonite at the base of the Chinglung Formation (Meishan section D), 5 cm above the paleontologically defined P-T boundary. This is the same bentonite from which previous dates of 251.2 ± 3.4 Ma (by U-Pb analysis of zircons) (19), 255.7 ± 0.4 Ma (by ⁴⁰Ar/³⁹Ar analysis of sanidine) (20), and 250 ± 6 Ma (by Rb/Sr analysis of sanidine) (20) have been reported. Sample GS-1 consisted of plagioclase grains (200 to 250 μ m across) from a bentonite in the Shangsi section, approximately 5 cm below the P-T boundary.

Incremental-heating ⁴⁰Ar/³⁹Ar analysis (21) of the Meishan sanidine (C-2) yielded a plateau date (Fig. 2A) of 249.91 ± 0.15

Ma (internal error) with an external error of ± 1.52 Ma. The mean date obtained by individual total-fusion analyses (Fig. 3A) is 249.62 Ma (± 0.30 Ma internal error; ± 1.54 Ma external error). This date is slightly younger than the step-heating plateau date, presumably because of subtle alterations whose effects are removed at low temperatures during step heating. Two separate incremental-heating analyses (21) of the Shangsi plagioclase (GS-1) yielded a combined weighted mean plateau date (Fig. 2, B and C) of 250.04 ± 0.36 Ma (internal error) with an external error of ± 1.13 Ma. The mean of individual grain total fusion dates (Fig. 3B) is 249.76 Ma (± 0.69 Ma internal error; ± 1.66 Ma external error); this is slightly younger than the weighted mean plateau age derived by incremental heating, again presumably because of cryptic alteration effects.

Because the two tuffs that yielded our samples are located just above and just below the P-T boundary and the dates we obtained from them are analytically indistinguishable, we estimate the age of the boundary itself to be equal to the mean of the two plateau dates, or 249.98 ± 0.20 Ma (internal error) with an external error of ± 0.95 Ma. This date can be compared with

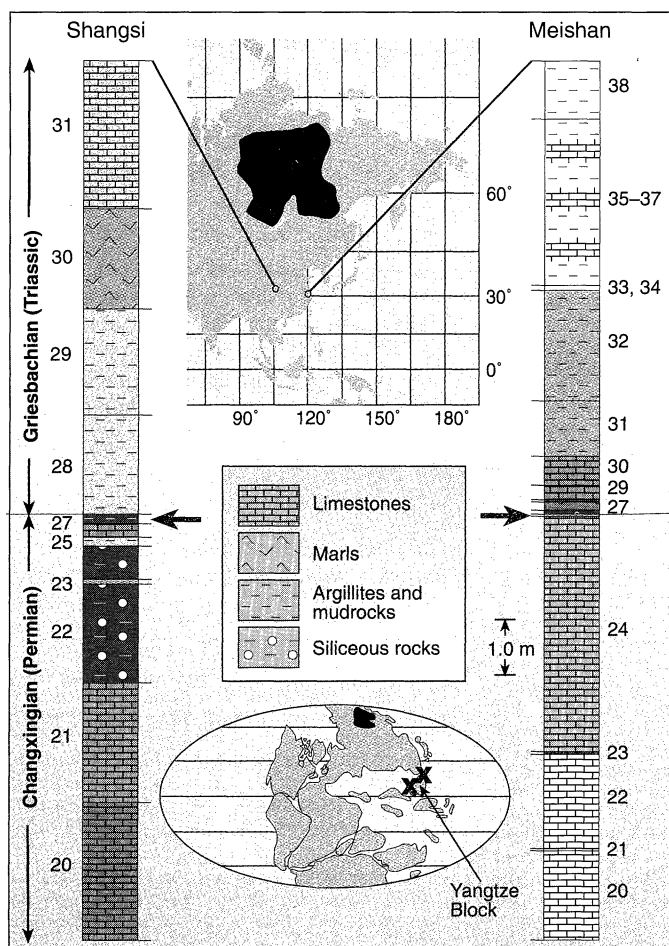


Fig. 1. Stratigraphic positions of the dated samples (red arrows) in the Shangsi and Meishan sections. The index map shows the present-day locations of the sections and the inferred original extent of the Siberian traps (black). The inset shows locations of the two sections (red X's) and the Siberian traps in a Pangaea reconstruction adapted from (10) at P-T time. Stratigraphy is based on (30) for the Shangsi section and on (19) and (31) for the Meishan section; in the stratigraphic columns, beds are numbered according to the original references, and colors (where shown) correspond to descriptions given in these references.

the Siberian traps on the basis of internal errors only, because uncertainty in the age of the fluence monitor is only a factor in determining absolute age. Thus the P-T boundary followed the initiation of main stage Siberian traps volcanism by 0.02 ± 0.36 My. A critical value test shows that these two dates can be distinguished at only the 6% confidence level.

The low probability of age difference between these two events strongly supports the notion of a causal relation between them. Siberian flood volcanism, perhaps augmented by sulfates derived from evaporites of the Siberian platform, could have produced sufficient stratospheric sulfate aerosols for rapid global cooling to ensue (11). Resulting ice cap accumulation likely caused the dramatic marine regression, which in turn led to sub-aerial exposure of the continental shelves. This latter effect would account for the ubiquitous anomalies in C, S, and Sr isotopes. Isotopically light C and S from mantle-derived CO₂ and SO₂ would also contribute to the observed negative anomalies in $\delta^{13}\text{C}$ and $\delta^{34}\text{S}$ (9). Ice storage effects plus enhanced erosion of the continental crust could have produced the seawater $\delta^{18}\text{O}$ enrichments observed at the boundary (22). Rapid transgression after the boundary would follow from the abrupt cessation of Siberian volcanism and the resulting ice cap recession. Climate recovery may have been enhanced by slower developing greenhouse effects of volcanogenic gases, primarily CO₂ (10).

Indeed, a short-lived volcanic winter, followed within several hundred thousand years by greenhouse conditions, would fully explain the environmental extrema that caused the P-T mass extinctions.

A complementary mechanism for the regression-transgression cycle centered on the P-T boundary involves the large-scale dynamics of the starting plume head that caused the Siberian flood volcanism. As a plume rises through the mantle, it causes an uplift of Earth's surface (23). The horizontal scale of this uplift is about 3000 km; this scale length is controlled mainly by the depth of the mantle rather than the size of the plume head, as long as the plume head is less than ~1500 km in diameter. This uplift collapses as the plume approaches the surface, spreads horizontally, and begins to produce large volumes of magma (24). Thus, the plume head model predicts a regression (uplift)-transgression (collapse) cycle of duration ~5 to 20 My, roughly centered in time on the flood basalt eruptions.

The central uplift over the plume head itself is expected to be ~1 to 3 km, which in the present case would have occurred over a ~500-km radius centered on the Siberian traps (24). On a broader scale of 3000 to 4000 km, dynamic flow calculations yield a regression-transgression amplitude on the order of 10 to 50 m, but the detailed spatial-temporal nature of this signal depends on the size of the plume and the detailed viscosity structure of the mantle beneath Siberia, neither of which is known. Thus it is possible that a considerable fraction of the Pangaeon landmass could have been lifted (and subsequently dropped) relative to sea level by as much as 50 m. Plume uplift might have also promoted the formation of a Siberian ice sheet at P-T time, because ice accumulation at high latitudes is very sensitive to continental elevation (25).

Such an ice sheet would lower the sea level globally, as in recent ice ages. Another plausible dynamic effect of the plume would be to induce rapid excursion of Earth's rotational axis from its normal geographic position, potentially causing "true polar wandering" (26) as it ascended quickly through the upper mantle. This could also have contributed to global climate disruption centered on the P-T boundary.

A marked decrease in seawater $^{87}\text{Sr}/^{86}\text{Sr}$ (to values <0.707) occurred immediately before the P-T boundary (9), as precipitously as the rapid rise at the boundary itself. Decreasing values of seawater $^{87}\text{Sr}/^{86}\text{Sr}$ indicate an increasing mantle-derived component, as would be caused by an increase in the production of mid-ocean ridge (MOR) basalts. However, heightened MOR activity at this time would produce a transgression rather than a regression; moreover, such activity appears unlikely because of the amalgamated nature of landmasses composing Pangaea at this time. It appears possible instead that isotopically primitive precursory Siberian magmatism represented in the Maimecha-Kotui subprovince, dated at 253.3 ± 2.6 Ma (27), initiated the decline in seawater $^{87}\text{Sr}/^{86}\text{Sr}$.

All of the aforementioned isotopic anomalies would have been enhanced by the occurrence of acid rain, an expected corollary effect of voluminous basaltic pyroclastic eruptions. The patterns of extinction of terrestrial floras at the boundary (that is, a "fern spike") are consistent with reduced insolation and a pulse of acid rain (8). The climatic impact of volcanogenic H₂SO₄ depends strongly on whether SO₂ gas and coalescing droplets are transported rapidly to the stratosphere. The abundance of pyroclastic volcanism in the Siberian traps, perhaps ~20% (11), provides a logical mechanism for disturbing the tropopause and transporting aerosol beyond the troposphere. The paleolatitude of the Siberian traps (60° to 80°N) was sufficiently high that polar lowering of the tropopause would have made the stratosphere significantly more accessible to volcanogenic aerosol input (5). Several researchers have concluded that the P-T mass extinctions were protracted (7) or occurred in several pulses (28) and that the formally recognized boundary represents only the dominant culmination of events. Such possibilities are consistent with the precursory Siberian (Maimecha-Kotui) magmatism discussed above, which was probably analogous to the earliest plume manifestations some 3 My before the main stage of Deccan magmatism in India (29).

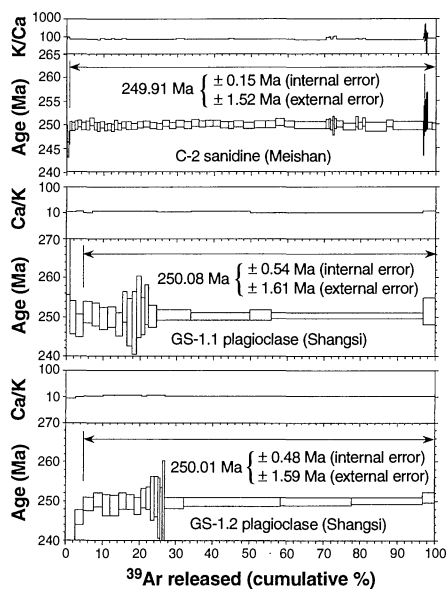


Fig. 2. Apparent age spectra and Ca/K or K/Ca ratios for laser incremental-heating analyses of three samples. The vertical height of the boxes represents 2σ intralaboratory error. The plateau ages were calculated for the indicated groups of steps; internal and external errors neglect and include, respectively, uncertainties in the age of the neutron fluence monitor.

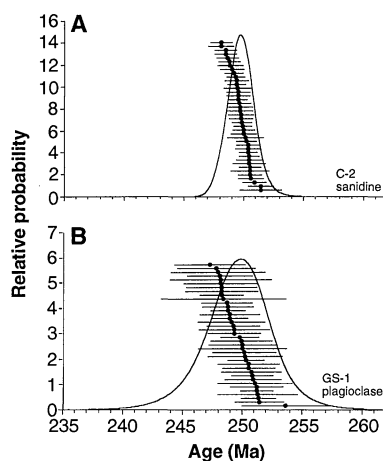


Fig. 3. Single-crystal apparent ages and age probability spectra (32) derived from laser total-fusion analysis of individual grains of feldspar from the samples indicated. Individual data are represented by black dots with 2σ internal error bars.

REFERENCES AND NOTES

1. M. A. Richards *et al.*, *Science* **246**, 103 (1989); R. S. White and D. P. McKenzie, *J. Geophys. Res.* **94**, 7685 (1989); I. H. Campbell and R. W. Griffiths, *Earth Planet. Sci. Lett.* **99**, 79 (1990); R. I. Hill *et al.*, *Science* **256**, 186 (1992).

2. D. M. McLean, *Cretaceous Res.* **6**, 235 (1985); C. B. Officer and C. L. Drake, *Science* **227**, 1161 (1985); V. E. Courtillot *et al.*, *Earth Planet. Sci. Lett.* **80**, 361 (1986); V. E. Courtillot, *Isr. J. Earth Sci.* **43**, 255 (1994).
3. M. R. Rampino, S. Self, R. B. Stothers, *Annu. Rev. Earth Planet. Sci.* **16**, 73 (1988).
4. R. B. Stothers, J. A. Wolff, S. Self, M. R. Rampino, *Geophys. Res. Lett.* **13**, 725 (1986).
5. H. Sigurdsson, *Geol. Soc. Am. Spec. Pap.* **247** (1990), p. 99.
6. D. M. Raup, *Science* **206**, 217 (1979); _____ and J. J. Sepkoski Jr., *ibid.* **231**, 833 (1986); D. H. Erwin, *Nature* **367**, 231 (1994).
7. D. H. Erwin, *Annu. Rev. Ecol. Syst.* **21**, 69 (1990); *The Great Paleozoic Crisis* (Columbia Univ. Press, New York, 1993).
8. G. J. Retallack, *Science* **267**, 77 (1995).
9. W. T. Holser and M. Magaritz, *Mod. Geol.* **11**, 155 (1987); *Geochim. Cosmochim. Acta* **56**, 3297 (1992). The notations $\delta^{13}\text{C}$ and $\delta^{34}\text{S}$ refer to $^{13}\text{C}/^{12}\text{C}$ and $^{34}\text{S}/^{32}\text{S}$ normalized to standard values, respectively.
10. J. J. Veever, P. J. Conaghan, S. E. Shaw, *Geol. Soc. Am. Spec. Pap.* **288** (1994), p. 187.
11. I. H. Campbell *et al.*, *Science* **258**, 1760 (1992).
12. M. Javoy and V. Courtillot, *Earth Planet. Sci. Lett.* **94**, 409 (1989); M. Palmer, *Nature* **352**, 758 (1991).
13. P. R. Renne and A. R. Basu, *Science* **253**, 176 (1991).
14. G. B. Dalrymple *et al.*, *Eos* **72**, 570 (1991); G. B. Dalrymple *et al.*, *Geochim. Cosmochim. Acta* **59**, 2071 (1995).
15. F. M. Gradstein *et al.*, *J. Geophys. Res.* **99**, 24051 (1994).
16. A. K. Baksi and E. Farrar, *Eos* **72**, 570 (1991).
17. P. R. Renne, *Earth Planet. Sci. Lett.* **131**, 165 (1995).
18. P. R. Renne *et al.*, *Geology* **22**, 783 (1994).
19. J. C. Clauoué-Long, Z. Zichao, M. Guogan, D. Shao-hua, *Earth Planet. Sci. Lett.* **105**, 182 (1991).
20. Z. Zichao, *Phanerozoic Time Scale Bull. Liais. Inform. IUGS Subcomm. Geochronol.* **10**, 14 (1992).
21. Samples were prepared at the Yichang Institute of Geology and Mineral Resources. Inspection of the samples under a polarizing microscope indicated that each was >99% pure. Samples were irradiated at the Oregon State University Reactor (Corvallis, OR) for 60 hours along with Fish Canyon sanidine (28.03 Ma) and MMhb-1 hornblende (523.4 Ma) neutron fluence monitors as well as synthetic materials to monitor nucleogenic interfering Ar isotope ratios; the latter were identical to previously reported values (17). Approximately 5 to 10 mg of sample for each run was analyzed by incremental heating of multigrain separates with a defocused argon-ion laser, with the use of facilities and procedures described previously (13, 17). Individual crystals from each tuff were analyzed by laser total fusion [A. L. Deino and R. Potts, *J. Geophys. Res.* **95**, 8453 (1990)]. Uncertainties in dates are reported at the 2σ level as both internal errors (neglecting uncertainty in the age of the neutron fluence monitor) and external errors (including uncertainty in the age of the monitor). Both plateau dates and mean dates of individual grain analyses are inverse variance weighted means. The Meishan sanidine (C-2) was analyzed in 65 steps of incremental degassing (Fig. 2A) and yielded a plateau over more than 99% of the ^{39}Ar released. The uniform K/Ca, derived from $^{39}\text{Ar}_K/^{37}\text{Ar}_{Ca}$ (Fig. 2A), attests to the mineralogical purity of the sample. Our new plateau date is significantly younger than the previous $^{40}\text{Ar}/^{39}\text{Ar}$ plateau date of 255.7 ± 0.4 Ma (20), probably because the two dates are based on different neutron fluence monitors that have not been intercalibrated. Because the previous $^{40}\text{Ar}/^{39}\text{Ar}$ experiment was performed on a sample of >100 mg, it was more likely to have contained xenocrystic contamination, although our new single-crystal data indicate that such contamination is unlikely. Forty individual grains of C-2 sanidine were also analyzed by laser total fusion. Dates calculated from the individual analyses show a symmetric and unimodal distribution (Fig. 3A) with no evidence of xenocrystic contamination. The Shangsi plagioclase (GS-1) was run in duplicate, with 20 steps in the first analysis (GS-1.1) and 21 steps in the second (GS-1.2). Both runs yielded well-defined plateaus over ~95% of the ^{39}Ar released (Fig. 2, B and C); the plateau dates and internal errors were 250.08 ± 0.54 and 250.01 ± 0.48 Ma, and external errors were ± 1.61 and ± 1.59 Ma, respectively. Uniform Ca/K is evident in both samples (Fig. 2, B and C). A combined weighted mean of the two plateau dates was calculated because the results from the two runs were indistinguishable at the 95% confidence level. Thirty-eight individual grains of GS-1 plagioclase were also analyzed by laser total fusion (Fig. 3B). The single-grain dates are more dispersed than those of C-2 sanidine, and uncertainties in individual results are larger, because of lower ^{40}Ar and ^{39}Ar signals relative to system background levels, but again the distribution is unimodal and not suggestive of xenocrystic contamination.
22. J. C. Hudson and T. F. Anderson, *Trans. R. Soc. Edinburgh Earth Sci.* **80**, 183 (1989).
23. M. A. Richards and B. H. Hager, *J. Geophys. Res.* **89**, 5987 (1984).
24. C. G. Farnetani and M. A. Richards, *ibid.* **99**, 13813 (1994).
25. G. E. Birchfield, J. Weertman, A. T. Lunde, *Quat. Res.* **15**, 126 (1981); G. E. Birchfield and M. Ghil, *J. Geophys. Res.* **98**, 10385 (1993).
26. Y. Ricard *et al.*, *Geophys. J. Int.* **113**, 284 (1993); M. A. Richards *et al.*, *Eos* **75**, 64 (1994).
27. A. R. Basu *et al.*, *Science* **269**, 822 (1995).
28. S. M. Stanley and X. Yang, *ibid.* **266**, 1340 (1994).
29. A. R. Basu *et al.*, *ibid.* **261**, 902 (1993).
30. L. Zishun *et al.*, *Study on the Permian-Triassic Biostratigraphy and Event Stratigraphy of Northern Sichuan and Southern Shaanxi* (Geological Publishing House, Beijing, 1989).
31. S. Jin-zhang *et al.*, *J. Fac. Sci. Hokkaido Univ. Ser. 4* **21**, 133 (1984); M. Ding, *Mem. Soc. Geol. Ital.* **34**, 263 (1986); K. Zhang, *Earth Sci. J. Wuhan Coll. Geol.* **12**, 193 (1987).
32. A. L. Deino and R. Potts, *Quat. Int.* **13**, 47 (1992).
33. Supported by NSF grants EAR-9496346 (P.R.R.), EAR-9117538 (M.A.R.), and EAR-9317214 (A.R.B.), the Ann and Gordon Getty Foundation (P.R.R. and M.T.B.), and the National Natural Science Foundation of China (Z.Z.). We thank T. A. Becker and W. D. Sharp for laboratory assistance and discussions and A. L. Deino, G. H. Curtis, and an anonymous reviewer for constructive reviews of the manuscript.

23 May 1995; accepted 12 July 1995

Short- and Intermediate-Range Structural Ordering in Glassy Boron Oxide

R. E. Youngman, S. T. Haubrich, J. W. Zwanziger,*
M. T. Janicke, B. F. Chmelka

Ordering at short-length scales is a universal feature of the glassy state. Experiments on boron oxide and other materials indicate that ordering on mesoscopic-length scales may also be universal. The high-resolution nuclear magnetic resonance (NMR) measurements of oxygen in boron oxide glass presented here provide evidence for structural units responsible for ordering on short- and intermediate-length scales. At the molecular level, planar $\text{BO}_{3/2}$ units accounted for the local ordering. Oxygen-17 NMR spectra resolved detailed features of the inclusion of these units in boroxol rings, oxygen bridging two rings, and oxygen shared between two nonring $\text{BO}_{3/2}$ units. On the basis of these and corroborative boron-11 NMR and scattering results, boron oxide glass consists of domains that are rich or poor in boroxol rings; these domains are proposed to be the structural basis of intermediate-range order in glassy boron oxide.

Inorganic network glasses such as B_2O_3 and SiO_2 lack long-range structural order, a physical property that differentiates them from analogous crystalline solids. However, glasses still have extensive short-range order (SRO) on length scales $< 5 \text{ \AA}$, and some exhibit substantial intermediate-range order (IRO) at 5 to 20 \AA (1). One such material is glassy boron oxide, B_2O_3 , which consists of planar $\text{BO}_{3/2}$ groups (that is, each boron is bound to three oxygen atoms, each of which is bound to another boron atom). The majority of the $\text{BO}_{3/2}$ groups are part of six-member boroxol rings that are interconnected to the rest of the $\text{BO}_{3/2}$ network by bridging oxygen atoms (Fig. 1). The remaining $\text{BO}_{3/2}$ units are not part of rings. The boroxol

ring is an example of what Elliott calls a superstructural unit, and it gives rise to IRO in this glass (2). Evidence for the boroxol ring structure has been obtained from neutron scattering (3), Raman spectroscopy (4), and NMR and nuclear quadrupole resonance (NQR) (5, 6). These experiments suggest that 70 to 80% of the boron is in the rings, which implies that the glass composition is a mixture of comparable amounts of boroxol rings and nonring $\text{BO}_{3/2}$ units. Bray and colleagues have also studied the oxygen sites in B_2O_3 glass, using continuous wave ^{17}O NMR (7). Their spectra could be fit to a two-site model, which is consistent with segregation of the oxygen between ring and nonring $\text{BO}_{3/2}$ units.

Recent light-scattering studies (8, 9) on a variety of glass formers, including B_2O_3 , suggest that IRO is universal at the glass transition. Moynihan and Schroeder have proposed that the anomalous light-scattering at the glass transition arises from independently relaxing structural units of linear

R. E. Youngman, S. T. Haubrich, J. W. Zwanziger, Department of Chemistry, Indiana University, Bloomington, IN 47405, USA.

M. T. Janicke and B. F. Chmelka, Department of Chemical Engineering, University of California, Santa Barbara, CA 93106, USA.

*To whom correspondence should be addressed.